# Experimental Research on a Honeycomb Microchannel Cooling System

Yonglu Liu, Xiaobing Luo, and Wei Liu

***Abstract*— A honeycomb porous microchannel cooling system for cooling electronics is proposed in this paper. The design, fabrication, and test system configuration of the microchannel heat sink are presented. Experiments were conducted to determine the heat transfer characteristics and cooling performance of this microchannel cooling system under steady single-phase flow of water. In the experiments, a brass microchannel heat sink was attached to a test heater with 8 cm$^2$ area. The heat transfer capabilities of the cooling system with different amounts of input heating power, different system designs, and various levels of pumping power were evaluated. The experimental results show that the designed cooing system performs well. For a heat sink design using double inlets and outlets, the system is able to remove a heat flux of 17.6 W/cm$^2$ under 0.72 W of pumping power, with the heater wall temperature of 61.4 °C and the ambient temperature of 17.8 °C. When the heat flux decreases to 9.4 W/cm$^2$ with the other conditions remaining the same, the heater substrate temperature is 42.4 °C. It is also clear from the experiments that the heat source temperatures are very uniform when cooled by the present system, which is important for many applications requiring high thermal reliability. As the pumping power and system flow rate increase, the heat source temperature sharply decreases. A heat flux of 18.2 W/cm$^2$ can be removed under 2.4-W pumping power when the heat source temperature is 48.3 °C and the ambient temperature is 14.9 °C.**

***Index Terms*— Electronics cooling, honeycomb, micro channel.**

## NOMENCLATURE

| | |
|---|---|
| $a$ | Seal region width around the microchannel plate perimeter. |
| $A$ | Area of the bottom wall of the microchannel heat sink. |
| $c_p$ | Specific heat. |
| $d$ | Honeycomb cell excircle diameter. |
| $D$ | Inner diameter of heat sink pipe. |
| $k$ | Thermal conductivity. |
| $H, W, L$ | Thickness, width, and length of microchannel plate. |
| $\dot{m}$ | Total mass flow rate. |
| $n$ | Number of microchannel plates. |
| $P$ | Input heating power. |
| $q$ | Heat flux at bottom wall of microchannel heat sink removed by liquid. |
| $\dot{Q}$ | Heat transfer rate removed by liquid. |
| $t$ | Honeycomb cell fin thickness. |
| $T$ | Temperature. |
| $\Delta T$ | Temperature change. |
| $\dot{v}$ | Total volumetric flow rate. |

Manuscript received May 19, 2009; revised December 19, 2010; accepted July 6, 2011. Date of publication August 30, 2011; date of current version September 21, 2011. This work was supported in part by the 973 Project of the Ministry of Science and Technology of China, under Program 2009CB320203, and also by New Century Excellent Talents Project of the Chinese Education Ministry under Project NCET-09-0387. Recommended for publication by Associate Editor P. Sathyamurthy upon evaluation of reviewers' comments.

The authors are with the School of Energy and Power Engineering, Huazhong University of Science and Technology, Wuhan 430074, China (e-mail: luoxb@hust.edu.cn).

Digital Object Identifier 10.1109/TCPMT.2011.2162331

## I. INTRODUCTION

As ELECTRONIC products are becoming faster and incorporating more functions, they are simultaneously shrinking in size and weight. These factors mean significant increases in the packing densities and heat fluxes for the electronic devices. Effective thermal management will be the key to ensure that these devices perform well with efficiency and reliability. The pioneering work of Tuckerman and Pease [1], [2] first introduced microchannel heat sinks for high heat flux applications, which have structures with many microscale channels of large aspect ratios. The heat sink they fabricated was able to dissipate 790 W from a 1-cm$^2$ silicon chip with a maximum substrate temperature rise of 71 °C and a pressure drop of 186 kPa. Following their original work, considerable research has been conducted on micro and mini heat sinks. Many of these studies focus on a single-layer plate fabricated from a highly thermally conductive solid, such as copper or silicon, with rows of small channels fabricated on their surfaces. A thorough review was presented by Sobhan and Garimella [3], and certain heat sink design methodologies, designs, and prototypical concepts were also presented in the review by John Goodling [4].

According to Newton's law of cooling, two conventional strategies can be employed to improve forced heat transfer rates under specified temperature difference for single-phase flow. One strategy involves extending the surface area of the heat sink. The use of microchannels here is attractive because of their compactness and high surface-to-volume ratio. However, the high packaging density in advanced electronic chips limits infinite extension of the heat sink surface area. In order to have high-aspect-ratio microchannel devices in a limited compact space, stacking or creating multiple layers of channels can be an alternative method in reducing the difficulties in fabrication. Vafai and Zhu [5] proposed a two-layer microchannel heat sink with a countercurrent flow arrangement. They found that the temperature increases and pressure drops along the two-layer microchannel structure were reduced compared to an equivalent single-layer heat sink. Wei and Joshi [6]–[8] analyzed a stacked microchannel heat

2156–3950/$26.00 © 2011 IEEE

sink that integrated many layers of liquid-cooled microchannels. Several layers of microchannels fabricated with silicon micromachining techniques were bonded into a stack. Because the stacked microchannels provided a larger heat transfer area, a significantly smaller amount of pumping power was required to remove heat at a certain rate than a single-layered microchannel. Patterson *et al.* [9] presented experimental and numerical work to investigate the characterization of one and two-layered Si microchannel heat sinks in parallel and counterflow configurations. They concluded that the counterflow configuration resulted in a more uniform surface temperature while the parallel flow configuration had a lower maximum surface temperature. Bower *et al.* [10] performed experimental studies on the heat transfer and pressure drop characteristics of single and multilayer silicon carbide heat sinks. They found that, despite its lower thermal conductivity, the heat sink performance compared favorably with that of single-layered copper heat sinks. Skandakumaran *et al.* [11] also proposed a multilayered microchannel heat sink by using an extrusion freeform fabrication technique. It was found that multilayer heat sinks had both lower thermal resistance and pumping power compared to single-layer samples, and their performance improved with the thermal conductivity of the heat sink material.

The other strategy to improve the forced conventional heat transfer rate is to enhance the heat transfer coefficient. While microchannel heat exchangers generally have excellent thermal performance, there is already considerable emphasis on increasing the heat transfer coefficients. For the long parallel fluid flow microchannels arrangement, the rise in coolant temperature is a result of the heat input along the flow direction. At the same time, because of the growing boundary layer, the heat transfer coefficients decrease along the flow direction. The use of enhanced microchannels was presented by Kishimoto and Sasaki [12]. They proposed a diamond-shaped interrupted microgrooved cooling fin to decrease the junction temperature variation across the chip. The high heat transfer coefficient was obtained by interrupting the thermal boundary layer with the staggered cooling fins. Steinke and Kandlikar [13] carried out an extensive review of conventional single-phase heat transfer enhancement techniques. Several passive and active enhancement techniques for mini channels and microchannels were discussed. Some of their proposed enhancement techniques include fluid additives, secondary flows, vibrations, and flow pulsations. Kandlikar and Upadhye [14] analyzed the enhanced offset strip-fin geometry. Their results showed that the enhanced structures were capable of dissipating heat fluxes extending beyond 3 MW/m$^2$ using water as the coolant in a split-flow arrangement with a core pressure drop of around 35 kPa. Jeung *et al.* [15] investigated the flow-induced vibration of a microfin array for heat transfer enhancement in laminar flow. Vibrating actuators had been introduced for active hydrodynamic mixing. The experimental results showed that the thermal resistance of the microfin array heat sink decreased by 11.5% compared to that of a plain-wall heat sink at an inlet air flow velocity of 5.5 m/s.

Recently, some researchers focused on honeycomb structures in augmenting heat transfer in compact heat exchangers. According to Lu [16], the surface area to volume ratio of the typical microcell aluminum honeycombs on the order of 1 mm was about 3000 m$^2$/m$^3$, making them ideal candidates for compact heat exchanger applications where high surface area density is required. Honeycomb structured metals are low-density materials that combine stiffness, strength, crushing energy absorption, and thermal characteristics. The continuous channels of these open-core structures with a single "easy flow" direction allows internal fluid transportation, which makes them particularly interesting for heat sink applications. For such reasons, all-metallic sandwich structures with honeycomb cores have been suggested for simultaneous load bearing and active cooling [17]. Several mechanisms contributing to heat transfer have been identified, including high surface area contact between the core and the coolant and high heat transfer between the metal surface and the fluid coolant [18]–[20]. Experimental studies of convective heat transfer in extruded metallic honeycomb structures have been performed by Hayes *et al.* [21] and Dempsey *et al.* [22]. The test heat sinks were fabricated as sandwich panels with honeycomb cores bonded by welding to two solid face-sheets, three sides insulated, and the top or bottom surfaces subjected to prescribed temperatures or heat fluxes using forced air as the coolant for the cross-flow heat exchange experiments.

Combining the characteristics of the multilayer channels structure with offset fins, we have designed a honeycomb microchannel heat sink in a cost-effective manner, as described in this paper. Multilayered metal plates each with rows of etched honeycomb cells were stacked to form staggered microchannels in the heat sink. Improved cooling performance was obtained based on the fluid hydrodynamic mixing improvements for periodic breakup of the thermal boundary layer. At the same time, the stacking structure design was easily implementable to obtain a higher surface-to-volume ratio in a limited space. It was expected that not only the surface area would expand, but the flow passage would also be modified to enhance the heat transfer efficiency. The design, fabrication, and test system configuration of the novel periodic staggered honeycomb microchannel heat sink are given in this paper. Experimental investigations were conducted to determine the heat transfer characteristics and cooling performance of the honeycomb microchannel cooling system. The system heat transfer performance was evaluated under various operational situations, including different microchannel heat sink parameters, test system configurations, and varied pumping power. The influence of the working flow rate and the test system on the cooling performance was also analyzed experimentally.

## II. Prototype of the Microchannel Heat Sink

The prototype of the stacked microchannel heat sink is comprised of an inner cellular metal core and an outer *Container*. The top view of one piece of the individual microchannel plate used in the heat sink inner core is shown in Fig. 1(a). The flat thin rectangular plate with length $L$, width $W$, and thickness $H$ is etched to have a number of small regular hexagonal honeycombs holes as seen in the figure. The seal region around the perimeter of the plate with no honeycombs is left for

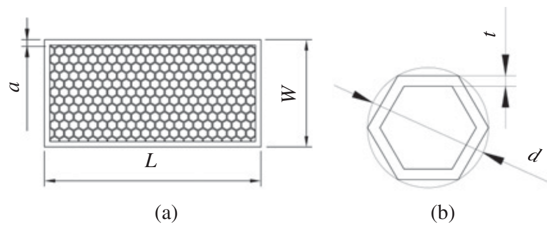


Fig. 1. Top view of one piece of the microchannel plates with regular hexagonal honeycombs. (a) Single layer. (b) One honeycomb hole.

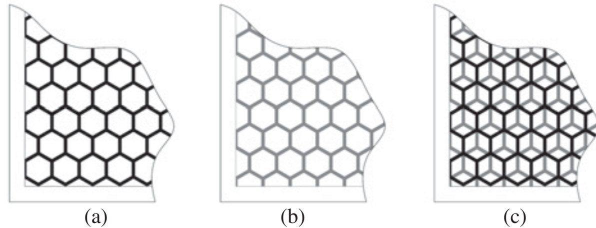


Fig. 2. Schematic view of the cellular metal core formation. (a) Layer 1. (b) Layer 2. (c) Bonded together.

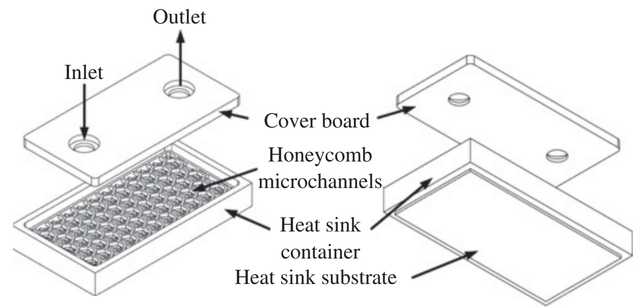


Fig. 3. Schematic of staggered honeycomb micro channel heat sink.

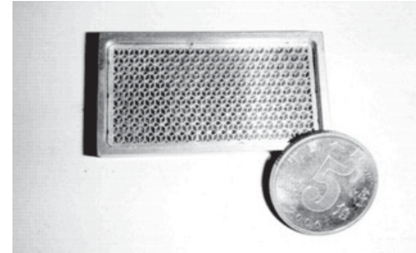

Fig. 4. Top view image of the interior of a honeycomb microchannel heat sink.

welding, its width is $a$. Each regular hexagonal honeycomb cell in the plate is described by the cell excircle diameter $d$ and the fin thickness $t$ as shown in Fig. 1(b).

Fig. 2 is a close-up view of one section of the individual honeycomb plate. Both layer 1 and layer 2 are completely of the same dimensions and have the same hexagonal honeycomb arrangement. Layer 2 is simply obtained by rotating layer 1 by 180 °C clockwise. As seen from Fig. 2, when stacking two layers of such honeycomb microchannel plates together, each honeycomb cell in layer 1 is divided into three smaller parts to form the offset-fin microchannels structure in layer 2. As multiple layers of such plates are bonded face to face with each other, the staggered array of honeycomb cells are created in the direction of the normal layer plane to form the heat sink inner cellular core. The heat sink *Container* is a concave chamber with the same dimensions as the inner cellular core and it is created using a high thermal conductivity metal material that facilitates heat flow from the bottom heat source into the sink. As shown in Fig. 3, when the cooling fluid enters and comes out from the cover board into the inner stacked plates with staggered honeycomb cells, a higher heat transfer coefficient and more uniform substrate surface temperature are obtained by the well-designed flow disturbance. Here, the heat sink substrate also has the same dimension of $L \times W$ as the inner microchannel plate.

The present heat sink design is different from the many usual sandwich structured honeycomb heat sinks mentioned above in that its inner cellular core is built by stacking multilayered honeycomb plates together and elaborately shaped by the honeycombs' regular intersection array. The fluid also flows in and out of the heat sink in the direction of the counterflow of the heat flux direction, which is different from the cross-flow direction in conventional honeycomb heat sinks.

The shapes of the hexagonal honeycomb plates are controlled well by a photochemical metal etching method. This is a method combining photochemical reactions with chemical corrosion. Initially, the metallic substrate is cleaned as well as possible to promote adhesion of the mask and retard undercutting during etching, then a strongly adhering etch-resistant mask is applied for the photoprocessing step of the coated metal. With CAD/CAM technology, processing figures are produced on the positive and negative mask plates. The protected metal part figures are formed on two sides of the positive and negative metal material through the photochemical reaction. Finally, the metal parts are produced through chemical etching of the unprotected metal material. The advantages of photochemical etching are the following: there are no burrs on the edges of the parts; the substrate is not subjected to heat or physical deformation; extremely small features can be obtained; the dimensions can be accurately controlled; and 2-D or 3-D parts can be etched. Modifications to the stencil can be done rapidly and relatively inexpensively, which results in a short time lapse between prototyping and production, and thus the cost of fabrication is also controlled.

In the present experimental work, the fabricated sample plate made of brass is $20 \times 40 \times 0.16$ mm in size and there is a 1-mm wide seal region around the perimeter with no honeycomb cells. The cell excircle diameter of the regular hexagonal honeycomb cell in the plate is 2.49 mm and its fin thickness is 0.2 mm, as indicated in Fig. 1(b). Such multilayered plates are stacked together to form the interior section of the heat sink. Although good metal bonding can minimize the contact heat resistance between two pieces of brass plates, in this paper, 15 pieces of the plates were joined together using laser welding on the side. The heat sink *Container* that houses the honeycomb microchannel structure is also made of brass, and the fluidic seals use miniature O-rings or laser welding. This honeycomb microchannel heat

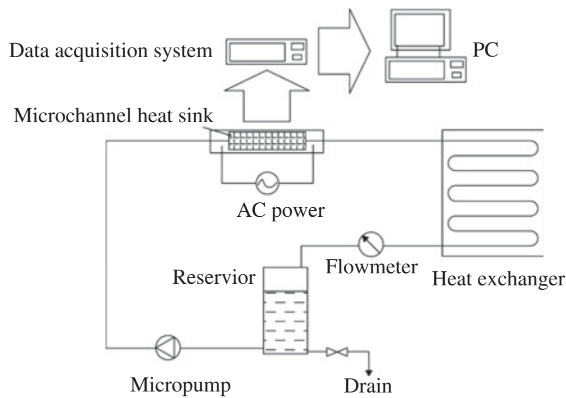


Fig. 5. Schematic of the honeycomb microchannel cooling system.

sink design combines the expectations that not only the surface area is expanded, but the improved flows are modified to enhance heat transfer in a cost-effective way. The top view of the inside fabricated sample is shown in Fig. 4. Heat is added to the bottom of the heat sink, and the working fluid flows in and out at the top surface.

## III. System Description and Experimental Setup

Fig. 5 shows the closed-loop honeycomb porous microchannel cooling test system. It is composed of four parts: a microchannel heat sink, a micropump, a reservoir, and a mini heat exchanger with fans. When electronic chips need to be cooled, the system starts to operate. Water in the closed system is driven into the heat sink device through the inlet located on the top surface of the heat sink by a micropump. The flow rate is controlled by adjusting the input voltage of the micropump. The water volumetric flow rate is monitored by a flow meter, which is calibrated using the standard weighing method, as follows. The liquid exiting the flow meter is collected in a glass beaker. A balance with an accuracy of ±1 g is used to weigh the accumulated liquid. The volume of the liquid is calculated by dividing the weight by the liquid's density.

In the system, the fluid is heated and its temperature increases after flowing out of the heat sink device. T-type thermocouples are located at the inlet and outlet of the test heat sink to measure the fluid temperatures at these locations. Through a 6-mm dia. tube, the heated fluid then enters the mini heat exchanger with fans. The mini heat exchanger will cool the fluid and the heat will be dissipated to the external environment. The cooled fluid will be delivered to the reservoir to ensure that the fluid entering the micropump is in the liquid phase and the micropump is working properly. From the low outlet of the reservoir, the cooled fluid is then pumped back into the heat sink, thus forming a closed-loop flow system. It should be noted that the real size of the system can be designed on the basis of the application requirements.

Fig. 6 shows a schematic cross-sectional view of the microchannel heat sink packaging. The test module is mounted at the center between two 8-mm thick thermally insulated cover plates. Heat was supplied using two 80-W cartridge heaters. The voltage input to the cartridge heaters is controlled by an ac power supply. Two small holes of 1-mm dia. are drilled to install two copper–constantan (T-type) thermocouples. Because of the good thermal conductivity of the copper material, the temperatures of the heat sink substrate are nearly equal to the measured ones. A thermal interface material (TIM) is used between the copper block heater surface and microchannel heat sink to minimize the contact heat resistance. In order to minimize heat loss, the external surface of the heater and the heat sink are all tightly covered with glass wool of a very low thermal conductivity ($k$ ~0.032 W/mK at 25 °C).

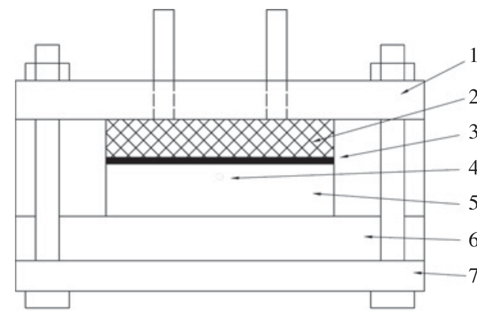


Fig. 6. Cross-section view of the microchannel heat sink package. 1-Top cover plate. 2-Microchannel heat sink. 3-TIM. 4-One thermocouple position. 5-Heater. 6-Thermal insulation board. 7-Bottom cover plate.

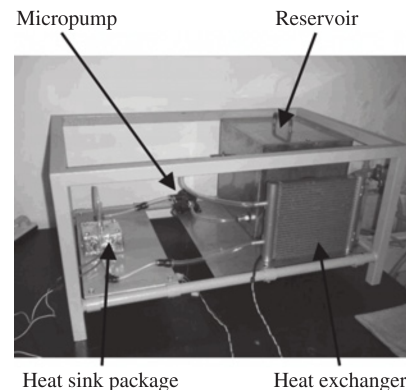


Fig. 7. Photograph of the experimental setup.

In the experiment, temperature is the main parameter for system evaluation, and it is directly measured using T-type thermocouples (Cu–CuNi). Calibration of the thermocouples is carried out before the experiment. The uncertainty of temperature measurement of the T-type thermocouples is ±0.2 K after calibration. All thermocouple output signals are recorded by a data acquisition system (Keithley 2700), which is connected to the PC via an RS232 port. The input heating power is controlled by the heating system, which is connected to a power supply with an adjustable ac voltage to provide power to the device. The uncertainty of the heating power measurement of the power meter is ±2 W. The electrical voltage and current of the micropump are respectively measured with a volt meter of ± 1V uncertainty and a current meter of ±0.1 A uncertainty.

For each test, the system was allowed to reach steady state before measuring and recording the liquid flow rate, liquid and heat sink substrate temperatures, as well as input voltage and current. All measured parameters were analyzed under steady-state conditions of the experiment. Two types of experimental

TABLE I
DIMENSIONS OF TEST HEAT SINKS

| Heat sink | $L$ (mm) | $W$ (mm) | $H$ (mm) | $a$ (mm) | $t$ (mm) | $d$ (mm) | $D$ (mm) | $n$ | Inlet | Outlet |
|---|---|---|---|---|---|---|---|---|---|---|
| \| | 40 | 20 | 0.2 | 3 | 0.2 | 2.27 | 2 | 8 | Single | Single |
| \|\| | 40 | 20 | 0.16 | 1 | 0.2 | 2.49 | 4 | 15 | Single | Single |
| \|\|\| | 40 | 20 | 0.16 | 1 | 0.2 | 2.49 | 4 | 15 | Double | Double |

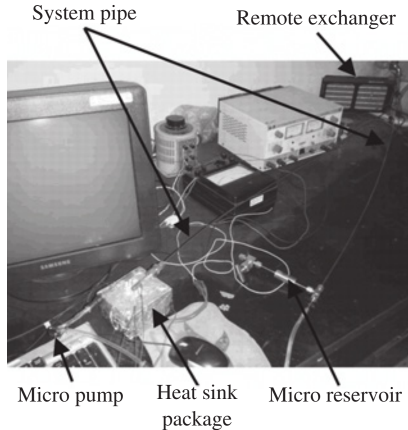


Fig. 8. Photograph of the remote micro-sized cooling system.

rig were set up as shown as in Figs. 7 and 8. Fig. 7 shows the practical cooling system described in Fig. 5. Fig. 8 shows the remote micro-sized heat transfer application cooling system, which includes a 2.3-m long stainless steel tube with only 2 mm inner diameter.

## IV. ANALYSIS AND DISCUSSION

During the experiments, the steady heat transfer rate $\dot{Q}$ removed by water and the corresponding heat flux $q$ at the substrate of the microchannel heat sink are given by

$$\dot{Q} = \dot{m} c_p \Delta T \tag{1}$$

$$q = \frac{\dot{Q}}{A} \tag{2}$$

where $\dot{m}$ is the total mass flow rate, $c_p$ is the specific heat of the fluid, and $\Delta T$ is the temperature change. The mass flow rate is calculated using the standard weighing method. The temperature change is determined from the measured inlet and outlet temperatures. $A$ is the substrate area of the microchannel heat sink. In this case, the substrate area is 8 cm$^2$.

In order to evaluate the cooling system, the power consumption of the micropump is also important. The electrical input power is determined by the expression

$$P = VI \tag{3}$$

where $V$ is the input voltage and $I$ is the input current.

The uncertainties of the experimental measurements were analyzed. The primary contribution for the margin of error of the total heat steady-state transfer rate $\dot{Q}$ was found to come from the temperature measurement. For the T-type thermocouples, the margin of error is about ±0.2 K after calibration, while the maximum margin of error for $\dot{Q}$ is 8.43%.

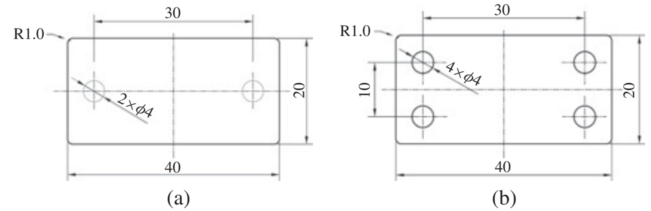


Fig. 9. Different heat sink cover configurations. (a) Single in/outlet. (b) Double in/outlet.

TABLE II
SPECIFICATIONS OF THE MICROPUMPS

| Micropump | Input voltage (V) | Current draw (A) | Power usage (W) | Pressure head (m) | Pipe size (inner diameter) (mm) |
|---|---|---|---|---|---|
| • | 12 | 2 | 24 | 3.1 | 12 |
| \|\| | 12 | 0.4 | 4.8 | 1.5 | 6 |
| \|\|\| | 3 | 0.28 | 0.84 | 1.1 | 3.2 |

Extensive experiments and analysis on the microchannel heat sinks integrated with cooling system configuration were conducted to examine how various operating conditions affected the thermal performance. Three test heat sinks were fabricated with different sizes, as listed in Table I. Heat sink ||| had the same dimension as the heat sink ||, but it had a double in/outlets cover arrangement. The detailed heat sink cover configurations are presented in Fig. 9. Because the heat sink *Container* was fabricated by milling, the cover edges were cut and formed with little filleted radius. Heat sink || also has single in/outlet cover arrangement, as shown in Fig. 9(a), but the diameter of the drilled holes was only 2 mm. Water was used as the coolant in single-phase experiments. Tests were conducted using various micropump types and pumping powers. The heat transfer capabilities of the cooling system with different pipe diameters and different input heating powers were also evaluated. The influence of working flow rate and test system configuration on the cooling performance was also analyzed experimentally.

When used as a compact cooling system for electronic chips, the pumping power of the micropump was required to be maintained at a low level. The nominal specifications of different micropumps used in the experiments are listed in Table II.

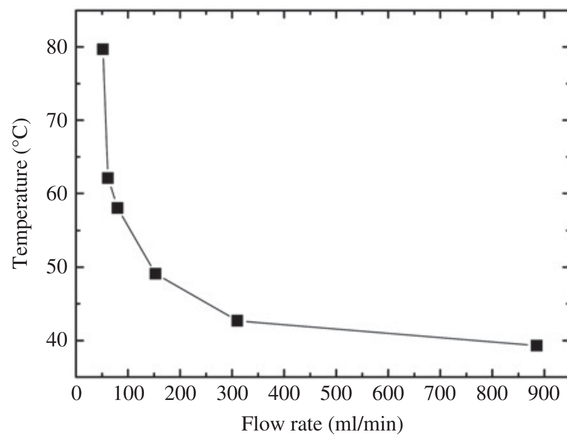


Fig. 10. Heat sink substrate temperature variation with different flow rates under 80-W heating power (heat sink I + micropump I).

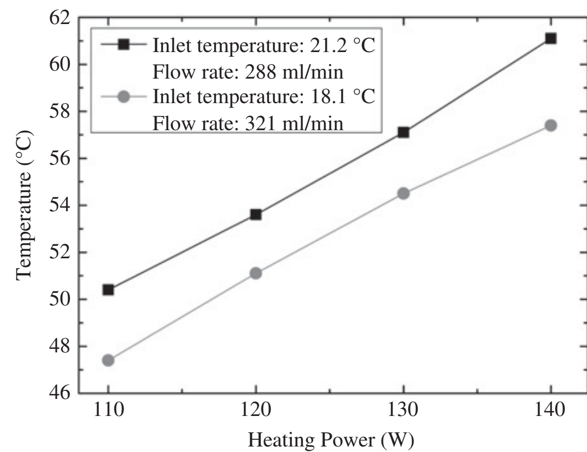


Fig. 11. Heat sink substrate temperature variation with input heating power at different inlet temperatures (heat sink I + micropump II).

Fig. 10. shows the relationship between heat sink substrate temperatures and volumetric flow rates under the same amount of heating power input with heat sink I and micropump I. The heat sink inlet water temperature was maintained at 21.2 °C in all tests. It can be seen that, as the flow rate increased, the substrate temperature decreased. When the system flow rate of the micropump was 885 ml/min, the substrate temperature was nearly 39.2 °C. However, when the flow rate decreased to 52 ml/min, the substrate temperature increased to about 80 °C. It is easy to explain this phenomenon. When the pumped flow rate increases, the average temperature of the coolant will decrease according to (1). The heat transfer coefficient of the porous honeycomb microchannel heat sink will also increase, thus the heat will be removed more efficiently. However, it should be noted that, as the pump flow rate increases, the micropump will also consume more power, which will increase the operational cost. In the present experiments, when the flow rate increases from 310 to 885 ml/min, the pumping power rises from 10 to 18 W. In actual practice, there should be some tradeoff in design between the heat transfer efficiency and the pump power consumption.

Another point that should be noted is the large difference in the connection pipe size between micropump I and the heat sink I. Micropump I has 12-mm inner diameter inlet and outlet pipes, but the heat sink I has 2-mm inner diameter inlet and outlet connection pipes. This means that when a sudden flow contraction or expansion appears at these places, significant hydrodynamic head losses will occur. Thus, a micropump with a small pipe is needed to fit the system pipe size, and the amount of pumping power also needs to be restricted to maintain a low level for microcooling applications. The micropump II with 6-mm inner diameter inlet and outlet pipes and 4.8-W nominal pumping power was introduced in the cooling system for evaluating the system performance.

Fig. 11 shows the variation of heat sink substrate temperatures with input heating power at different inlet water temperatures using heat sink I and micropump II. Here, tests were conducted at two different inlet water temperatures using the same amount of pumping power. The average flow rates were 298 ml/min under 21.2 °C inlet water and 322 ml/min under 18.1 °C. Because the density of water changes with temperature, the flow rate is slightly lower with a higher inlet fluid temperature. In the tests, the substrate temperatures increased with the rise of the input heating power. Under conditions of 21.2 °C inlet temperature and 288 ml/min flow rate, the substrate temperature was about 50.4 °C under 110 W, and increased to 61.1 °C as the heating power rose to 140 W. In this case, 129 W of heating power was effectively removed by the water flow according to (1). When the inlet temperature was 18.1 °C and the flow rate was 321 ml/min, the substrate temperature was about 47.4 °C under 110 W and increased to 57.4 °C as the heating power rose to 140 W. From Fig. 11, it can be seen that improved cooling capabilities of the system were achieved with lower inlet water temperatures under constant pumping power.

Although a large flow rate and low working fluid temperature can improve the system's cooling performance, in many electronic heat removal applications the micropump's working parameters are always maintained constant. That means that, in order to obtain larger flow rate for better cooling performance, the only way is to decrease the system flow resistance. Heat sink I was designed to reduce flow hydrodynamic head losses. Compared to heat sink I, it had a larger honeycomb cell and a smaller seal region. Most significantly, the inner diameter of the in/outlet pipes of heat sink I was 4 mm, which is 2 mm larger than that of heat sink I.

More details of the two types of heat sinks can be seen in Table I. The effect of these two different heat sink designs on the substrate temperature under the same amount of pumping power is shown in Fig. 12. Using the same micropump II and constant 2.4 W (dc 12 V, 0.2 A) pumping power, two types of heat sinks were tested under 16.2 °C inlet water temperature. It is clear from Fig. 10 that the flow rate of heat sink II was much higher than that of heat sink I, which shows that this design results in lower flow resistance because of the larger honeycomb cell size and in/outlet pipe diameter. For the cooling system, the substrate temperature was 47.2 °C with heat sink I and 110 W input heating power, which is 5 °C higher than

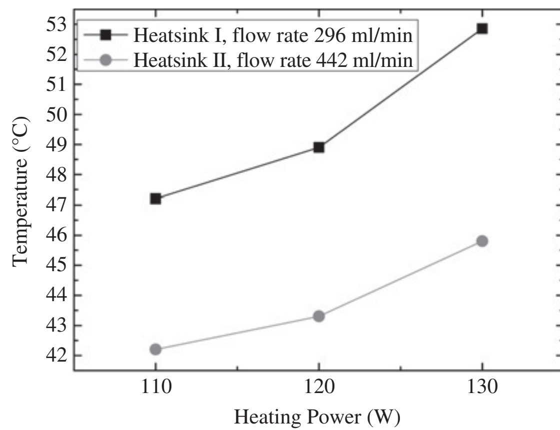


Fig. 12. Heat sink substrate temperature variation with input heating power at different heat sink designs.

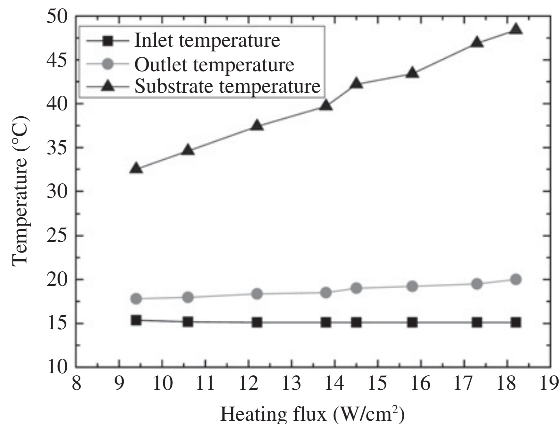


Fig. 13. Temperature variation with time at different heating powers (heat sink ‖ + micropump ‖).

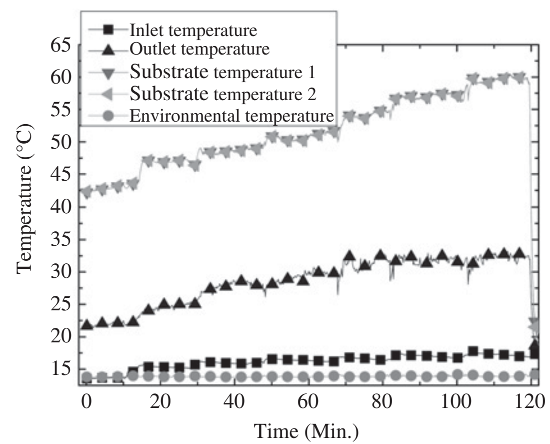


Fig. 14. Temperature variation with time at different input heating power (heat sink ‖ + micropump ‖).

that with heat sink ‖. When the heating power rose to 130 W, the substrate temperature of heat sink | increased to 52.8 °C, i.e., 7 °C higher than that with heat sink ‖ as shown in Fig. 12.

Detailed tests were conducted with heat sink ‖ and micropump ‖ at various input heating power levels. Fig. 13 shows the heat sink temperature variations with time at different heat fluxes in steady flow rate. Here, the average flow rate was 463 ml/min and the ambient temperature was 14.9 °C. The input voltage and current to the pump were kept at dc 12 V and 0.2 A, respectively, thus the pump power consumption was 2.4 W. The tests were initially started using 80 W of heating power, and then stepped up to 90, 100, 110, 120, 140, and finally, 150 W. From Fig. 13, it can be seen that, when the input heating power was 80 W, the inlet water fluid temperature was 15.3 °C, the outlet temperature was 17.8 °C, and the substrate temperature of the heat sink was 32.5 °C. Thus the total heat transfer rate $\dot{Q}$ removed by water calculated using (1) was 75.2 W, and the heat flux $q$ at the substrate of the microchannel heat sink removed by water was 9.4 W/cm$^2$ based on (2), as shown in the right $y$-axis of Fig. 13. When the input heating power was increased to 150 W, the inlet water fluid temperature was 15.1 °C, the outlet temperature was 20 °C, and the substrate temperature of the heat sink rose to 48.3 °C, which was safe enough for normal electronic chips. In this case, the total heat transfer rate $\dot{Q}$ was 145.6 W, and the heat flux $q$ at the substrate of the microchannel heat sink removed by water was 18.2 W/cm$^2$. Actually, a higher amount of heat could be removed by the cooling system, but in this experimental system the design had a restriction with a maximum of 160 W input power, which limited further experiments. It was also found that, when the heating system stopped heating, the substrate temperature decreased rapidly to the ambient temperature.

For remote micro-sized heat transfer applications, the system will need to further minimize its configuration dimensions to fit into the limited space. As shown in Fig. 7, the 2.4-m long stainless steel tubes with only 2-mm inner diameter were used as the system fluid pipes to transfer the heat generated by the electronics through a distance of 1.2 m. Thus great flow resistance will be generated in these tiny long pipes, which would limit the system flow rate to a very low level. On the other side, as system components are miniature, there is also a need to restrict the micropump's size, which means that a smaller micropump is required with lower power consumption. It should further reduce the heat sink flow resistance for applications in such conditions. Compared to heat sink ‖, heat sink ‖| had double in/outlet pipes arrangement, with the benefit of multiple passes with shorter flow lengths to reduce the flow resistance. Micropump ‖| with a small pipe size of 3.2 mm inner diameter and low working voltage of 3 V was used to push water through the cooling system.

Fig. 14 shows the variations of the heat sink temperature with time at different input heating powers at steady flow rate. During the experiments, the flow rate of the micropump was 105 ml/min and the ambient temperature was 13.9 °C. The consumed power of the micropump ‖| was 0.72 W (dc 3 V, 0.24 A). The input power increased from 80 to 140 W, in 10 W per stage. When the input power was 80 W, the corresponding heat flux was 9.4 W/cm$^2$ and the substrate temperature of the heat source was 42.5 °C. It can also be found that the two measured substrate temperatures were nearly the same, which indicated the uniformity of temperature distribution in the heat sink substrate. This is very important for those applications that need low thermal stress and high reliability.

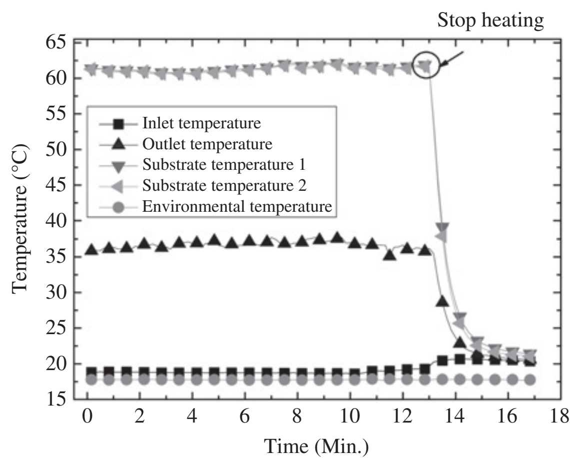


Fig. 15. Temperature variation with time at 150-W input heating power (heat sink ||| + micropump |||).

Fig. 15 shows the measured temperature variation with time at 150 W input heating power. In this case, the flow rate was 115 ml/min, the power consumption was 0.72 W (dc 3 V, 0.24 A), the ambient temperature was 17.8 °C, the inlet water fluid temperature was 18.9 °C, outlet temperature was 36.6 °C, and the substrate temperature of the heat sink rose to 61.4 °C and 61.2 °C. According to (1) and (2), the total heat transfer rate $\dot{Q}$ was 142 W, and the heat flux $q$ at the substrate of the microchannel heat sink was 17.7 W/cm$^2$.

## V. Conclusion

A practical implementation of a single-phase brass honeycomb porous microchannel cooling system was developed for cooling electronic chips. Metal etching was used for the fabrication, in which the cooling fluid entered in and out from the top side of the cascaded plates with staggered honeycomb cells. Good heat transfer was obtained by an improved design for flow disturbance. Experimental investigations were conducted to determine the heat transfer characteristics and cooling performance under steady single-phase flow. Different heat sink designs and micropumps with various operation parameters were tested. The experimental results showed that the cooling system could remove a heat flux of 18.2 W/cm$^2$ under 2.4 W of pumping power, when the heat source temperature was 48.3 °C and the ambient temperature was 14.9 °C. This heat sink design provides an excellent choice for cooling electronic chips.

## References

[1] D. B. Tuckerman and R. F. W. Pease, “High-performance heat sinking for VLSI,” *IEEE Electron Dev. Lett.*, vol. 2, no. 5, pp. 126–129, May 1981.
[2] D. B. Tuckerman and R. F. W. Pease, “Optimized convective cooling using micromachined structure,” *J. Electrochem. Soc.*, vol. 129, no. 3, p. C98, 1982.
[3] C. B. Sobhan and S. V. Garimella, “A comparative analysis of studies on heat transfer and fluid flow in microchannels,” *Microscale Thermophys. Eng.*, vol. 15, no. 4, pp. 293–311, 2001.
[4] J. Goodling, “Microchannel heat exchangers: A review,” *Proc. SPIE: High Heat Flux Eng. II*, vol. 1997, pp. 67–82, Jul. 1993.
[5] K. Vafai and L. Zhu, “Analysis of two-layered micro-channel heat sink concept in electronic cooling,” *Int. J. Heat Mass Transf.*, vol. 42, no. 12, pp. 2287–2297, Jun. 1999.
[6] X. Wei and Y. Joshi, “Stacked microchannel heat sinks for liquid cooling of microelectronic components,” *J. Electron. Packag.*, vol. 126, no. 1, pp. 60–66, Mar. 2004.
[7] X. Wei and Y. Joshi, “Optimization study of stacked micro-channel heat sinks for micro-electronic cooling,” *IEEE Trans. Comp. Packag. Technol.*, vol. 26, no. 1, pp. 55–61, Mar. 2003.
[8] X. Wei, Y. Joshi, and M. K. Patterson, “Experimental and numerical study of a stacked microchannel heat sink for liquid cooling of microelectronic devices,” *J. Heat Transf.*, vol. 129, no. 10, pp. 1432–1444, Oct. 2007.
[9] M. K. Patterson, X. J. Wei, Y. Joshi, and R. Prasher, “Numerical study of conjugate heat transfer in stacked microchannels,” in *Proc. 9th Intersoc. Conf. Thermal Thermomech. Phenom. Electron. Syst.*, vol. 1. Las Vegas, NV, Jun. 2004, pp. 372–380.
[10] C. Bower, A. Ortega, P. Skandakumaran, R. Vaidyanathan, and T. Phillips, “Heat transfer in water-cooled silicon carbide milli-channel heat sinks for high power electronic applications,” *J. Heat Transf.*, vol. 127, no. 1, pp. 59–65, Jan. 2005.
[11] P. Skandakumaran, A. Ortega, T. Jamal-Eddine, and R. Vaidyanathan, “Multilayered SiC microchannel heat sinks - modeling and experiment,” in *Proc. 9th Intersoc. Conf. Thermal Thermomech. Phenom. Electron. Syst.*, vol. 1. Jun. 2004, pp. 352–360.
[12] S. Sasaki and T. Kishimoto, “Optimal structure for microgrooved cooling fin for high-power LSI devices,” *Electron. Lett.*, vol. 22, no. 25, pp. 1332–1334, Dec. 1986.
[13] M. E. Steinke and S. G. Kandlikar, “Single-phase heat transfer enhancement techniques in microchannel and minichannel flows,” in *Proc. 2nd Int. Conf. Microchannels Minichannels*, Rochester, NY, Jun. 2004, pp. 141–148.
[14] S. G. Kandlikar and H. R. Upadhye, “Extending the heat flux limit with enhanced microchannels in direct single-phase cooling of computer chips,” in *Proc. IEEE 21st Annu. Semicond. Thermal Meas. Manag. Symp.*, San Jose, CA, Mar. 2005, pp. 8–15.
[15] J. S. Go, S. J. Kim, G. Lim, H. Yun, J. Lee, I. Song, and E. Pak, “Heat transfer enhancement using flow-induced vibration of a microfin array,” *Sens. Actuat. A: Phys.*, vol. 90, no. 3, pp. 232–239, May 2001.
[16] T. J. Lu, “Heat transfer efficiency of metal honeycombs,” *Int. J. Heat Mass Transf.*, vol. 42, no. 11, pp. 2031–2040, Jun. 1999.
[17] A. G. Evans, J. W. Hutchinson, and M. F. Ashby, “Multifunctionality of cellular metal systems,” *Progr. Mater. Sci.*, vol. 43, no. 3, pp. 171–221, Jul. 1999.
[18] T. J. Lu, L. Valdevit, and A. G. Evans, “Active cooling by metallic sandwich structures with periodic cores,” *Progr. Mater. Sci.*, vol. 50, no. 7, pp. 789–815, Sep. 2005.
[19] J. Tian, T. J. Lu, D. T. Queheillalt, and H. N. G. Wadley, “Cross flow heat exchange of textile cellular metal core sandwich panels,” *Int. J. Heat Mass Transf.*, vol. 50, nos. 13–14, pp. 2521–2536, 2007.
[20] T. Wen, J. Tian, T. J. Lu, D. T. Queheillalt, and H. N. G. Wadley, “Forced convection in metallic honeycomb structures,” *Int. J. Heat Mass Transf.*, vol. 49, nos. 19–20, pp. 3313–3324, Sep. 2006.
[21] A. M. Hayes, A. Wang, B. M. Dempsey, and D. L. McDowell, “Mechanics of linear cellular alloys,” *Mech. Mater.*, vol. 6, no. 8, pp. 691–713, Aug. 2004.
[22] B. M. Dempsey, S. Eisele, and D. L. McDowell, “Heat sink applications of extruded metal honeycombs,” *Int. J. Heat Mass Transf.*, vol. 48, nos. 3–4, pp. 527–535, Jan.–Feb. 2005.

**Yonglu Liu** received the M.S. degree in mechanical engineering from the Huazhong University of Science and Technology (HUST), Wuhan, China. He is currently pursuing the Ph.D. degree with HUST.

His current research interests include heat and mass transfer and microcooling.

**Xiaobing Luo** received the Ph.D. degree from Tsinghua University, Beijing, China, in 2002.

He was with Samsung Electronics, Seoul, Korea, as a Senior Engineer, from 2002 to 2005. In September 2005, he returned to China and joined the Huazhong University of Science and Technology (HUST), Wuhan, China, as an Assistant Professor. In October 2007, he was promoted to Full Professor. He is currently with the School of Energy and Power Engineering and the Wuhan National Laboratory for Optoelectronics, HUST. He has published more than 50 research papers, and has applied for or been awarded 40 patents in the U.S., Korea, Japan, Europe, and China. His current research interests include light emitting diode packaging, electronics packaging, heat and mass transfer, microelectromechanical systems sensors, and actuators.

**Wei Liu** is a Professor at the Huazhong University of Science and Technology (HUST), Wuhan, China. He is with the School of Energy and Power Engineering, HUST. He has published more than 100 papers and has applied for or been awarded 10 patents in China. His main research interests include heat and mass transfer.